Erbium fiber laser–pumped continuous-wave microchip Cr^{2+}:ZnS and Cr^{2+}:ZnSe lasers

S. B. Mirov, V. V. Fedorov, K. Graham, and I. S. Moskalev

Laser & Photonics Research Center, Department of Physics, The University of Alabama at Birmingham, 1300 University Boulevard, Birmingham, Alabama 35244-1170

V. V. Badikov and V. Panyutin

Kuban State University, 149 Stavropolskaya Street, Krasnodar 350040, Russia

Received October 2, 2001

Efficient continuous-wave (cw) lasing of Cr^{2+}:ZnS and Cr^{2+}:ZnSe crystals in external hemispherical cavities and in a microchip configuration under Er-fiber-laser pumping at room temperature are reported. The key result is what is believed to be the first successful demonstration of cw Cr^{2+}:ZnS and Cr^{2+}:ZnSe microchip lasers with maximum output powers of 63 and 100 mW at 2320 and 2520 nm, with slope efficiencies of 53% and 20%, respectively. © 2002 Optical Society of America

OCIS codes: 140.3070, 140.5680, 140.3500.

There is a growing demand for affordable, compact, room-temperature operational and broadly tunable mid-IR laser sources for use in a variety of remote-sensing applications. DeLoach *et al.*[1] and Page *et al.*[2] recently performed detailed spectroscopic studies of several II–VI chalcogenide hosts with different divalent transitional-metal ions (TM^{2+}) as potential mid-IR laser materials. Since then, laser demonstrations over the 2–3-μm spectral region in continuous-wave (cw) free-running long-pulse, Q-switched, and mode-locked regimes of operation were reported for Cr:ZnS,[3,4] Cr:ZnSe,[5–8] Cr:$Cd_{1-x}Mn_xTe$,[9] and Cr:CdSe (Ref. 10) crystals. A key feature of these materials is low energy of the optical photon cutoff, which decreases the efficiency of nonradiative decay and promises a high yield of fluorescence at room temperature.

In this Letter we extend our effort to develop high-optical-density and high-quality Cr^{2+}:ZnS and Cr^{2+}:ZnSe crystals synthesized by chemical transport reaction from the gas phase and activated by a diffusion doping method.[3,4] The key objectives of the research have been to provide the first demonstration of cw lasing of Cr^{2+}:ZnS crystals and specifically to investigate the feasibility of lasing of Cr^{2+}:ZnS and Cr^{2+}:ZnSe crystals in a microchip configuration under cw Er-fiber-laser pumping. Microchip lasers are important candidates for cost-effective and compact lasers with very short cavity lengths (from a few hundred micrometers to a few millimeters).[11]

The room-temperature absorption and emission spectra of Cr^{2+}:ZnS and Cr^{2+}:ZnSe crystals, corrected for the detection system's spectral response, are shown in Fig. 1. The maximum absorption coefficients of the studied crystals at room temperature were $\alpha = 10\ cm^{-1}$ (at $\lambda = 1690$ nm) and $\alpha = 12\ cm^{-1}$ (at $\lambda = 1770$ nm) for Cr^{2+}:ZnS and Cr^{2+}:ZnSe crystals, respectively. The Cr^{2+} concentrations in these crystals as estimated from absorption measurements[3,4] were $\sim 14 \times 10^{18}\ cm^{-3}$ and could vary in some crystals with different thermodiffusion conditions from 10^{18} to $10^{20}\ cm^{-3}$ without noticeable concentration quenching.

The pump source for the laser experiments was an Er-doped fiber laser (ELD-2, IPG Photonics). The laser delivered 2 W of single-mode cw nonpolarized radiation at 1550 nm and was equipped with an optical isolator that prevented feedback from the ZnS and ZnSe laser resonators. The fiber core was 10 μm in diameter. For external nonselective resonator laser experiments, the hemispherical cavity consisted of flat input and concave (20-cm radius-of-curvature) output mirrors. The input-mirror crystal had 99.5% reflectivity in the 2.2–2.5-μm spectral region. The output mirrors had 2–20% transmission in the 2.2–2.5-μm spectral region. Laser experiments were performed on the crystals doped from the gas phase. An antireflection-coated Cr^{2+}:ZnS

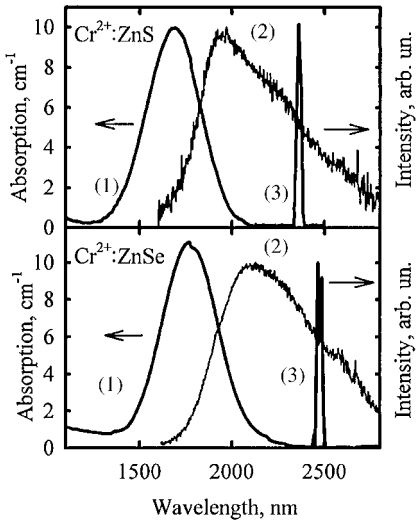

Fig. 1. (1) Room-temperature absorption, (2) emission [in W/(nm/m^2)], and (3) laser oscillation spectra of Cr^{2+}:ZnS and Cr^{2+}:ZnSe crystals.

0146-9592/02/110909-03$15.00/0

crystal with a thickness of 1.1 mm and an absorption coefficient of 5 cm^{-1} at the pump wavelength was utilized. The crystal was mounted directly on the flat dichoric input mirror, which was made from YAG crystal for effective heat dissipation. The pump radiation of the Er fiber laser was first collimated with a microscope objective ($f = 4$ mm) and then focused with a second 15-mm focal-length objective into the crystal though the input mirror. The output laser parameters were different when the output coupler and the cavity length were adjusted to minimum threshold or maximum output power. The difference between these adjustments is associated with a change of the mode volume because of thermal lensing in the gain medium. The output–input dependences of Cr^{2+}:ZnS cw lasing under Er-fiber pumping for two different output couplers and for different cavity adjustments to the minimum threshold and maximum output power are depicted in Fig. 2.

The minimum threshold values were 100 and 220 mW of absorbed pump power for output couplers with 2% and 20% transmission, respectively. An output power of 63 mW near 2360 nm at an absorbed pump power of 0.6 W was demonstrated with a 2% transmission output coupler at the maximum output-power adjustment. The maximum slope efficiency, η, with respect to the absorbed pump power was 18% in this experiment for the adjustment to the maximum output power. The oscillation linewidth in the nonselective cavity was 50 nm. The round-trip passive losses (L) in the cavity were estimated from a Findley–Clay analysis to be 3.7%.[12] The limiting slope efficiency of the studied crystal was estimated to be 51% from analysis[13] of slope efficiency versus output coupling with the equation

$$\eta = \eta_0 T/(L + T), \qquad (1)$$

where η is the slope efficiency, η_0 is the limiting slope efficiency, and T is the mirror transmission. This value is close to the quantum defect of 65% for the studied crystal. Note that the oscillation wavelength was significantly shifted with respect to the maximum of the Cr^{2+}:ZnS luminescence band [curve (1), top part of Fig. 1]. This shift was due to the shift of the gain with respect to the luminescence to longer wavelengths and the available cavity mirrors utilized in this experiment, which had maximum reflectivity in the 2300–2400-nm spectral range.

Microchip laser experiments were performed on both Cr^{2+}:ZnS and Cr^{2+}:ZnSe crystals. The crystals were polished flat and parallel (parallelism of ~10 arc sec) to 1.0- and 2.5-mm thickness, respectively. The mirrors were directly deposited on parallel polished facets of a thin wafer of laser material. The input and output dichroic mirrors had 0.01% and 3.5% transmission, respectively, over the 2300–2500-nm spectral region. Two different pump arrangements were utilized. The first was identical to the pump conditions for the Cr^{2+}:ZnS cw lasing in a hemispherical cavity. The second pump arrangement was provided without any coupling optics by means of a microchip laser mounted close (~20 μm) to the tip of the pump Er-fiber laser. Figure 3 shows the output power of the Cr^{2+}:ZnS and Cr^{2+}:ZnSe microchip lasers plotted as a function of absorbed pump power.

In a focused pump-beam arrangement a laser threshold of 120 mW and a slope efficiency of 53% with respect to the absorbed pump power were realized for the Cr^{2+}:ZnS microchip laser. The high (close to the theoretical limit of 65%) slope efficiency of the microchip laser indicates that the crystal is high quality with low loss. The maximum output power reached 63 mW. Thermal effects provided cavity stabilization within the microchip crystals and are responsible for the slightly nonlinear character of the output versus the input laser performance. In the case of ZnSe microchip lasing, in a focused pump-beam arrangement a laser threshold of 190 W with a slope efficiency of 20% with respect to the absorbed pump power was demonstrated. The maximum output power reached 100 mW.

In the second pump arrangement, when the microchip lasers were directly coupled to the fiber tip, laser thresholds of 150 and 240 mW and slope efficiencies of 36% and 14% with respect to the absorbed pump power were realized for Cr^{2+}:ZnS and Cr^{2+}:ZnSe microchip lasers, respectively. The maximum output power of the Cr^{2+}:ZnS microchip laser was practically

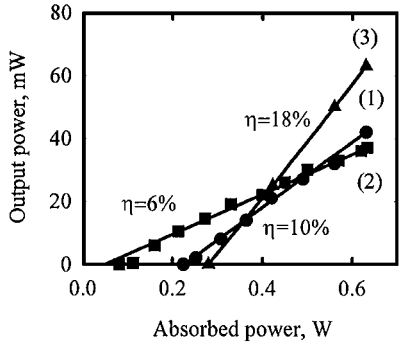

Fig. 2. Output–input characteristics of the Cr^{2+}:ZnS cw lasers under 1.55-μm Er-fiber-laser pumping with difference output couplers: (1) $T = 20\%$ and (2) $T = 2\%$ correspond to minimum threshold adjustment, (3) $T = 2\%$ corresponds to adjustment to maximum output power. The slope efficiencies, η, are labeled.

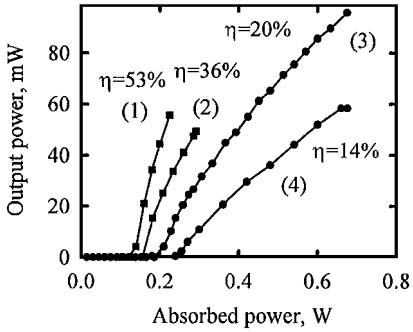

Fig. 3. Output–input characteristics of the (1), (2) Cr^{2+}:ZnS and (3), (4) Cr^{2+}:ZnS cw microchip lasers under Er-fiber-laser excitation. (1), (3) focused pump-beam arrangement; (2), (4) no coupling optics between the fiber tip and the microchip.

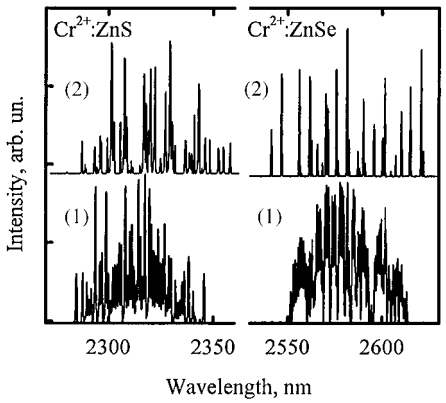

Fig. 4. Mode structures of the (1) microchip lasers and (2) coupled-cavity microchip lasers (with external etalons) for Cr^{2+}:ZnS and Cr^{2+}:ZnSe crystals.

unchanged in either pump arrangement, whereas for Cr^{2+}:ZnSe it dropped by a factor of 1.6 when it was directly coupled to the fiber tip compared with the focused pump arrangement. This drop can be explained by the excessive length and corresponding mismatch in the mode size and the pump-beam profile of the ZnSe microchip.

The output spectra in free-running laser operation covered the 2280–2350- and 2550–2620-nm spectral ranges for ZnS and ZnSe microchip lasers, respectively. At the maximum pump power the output spectrum of the Cr^{2+}:ZnSe laser consisted of more than 100 axial modes, with a free spectral range $\Delta\nu = 1.3\ \mathrm{cm}^{-1}$. The typical output spectra of the microchip lasers are depicted by traces (1) of Fig. 4. Because of its smaller crystal thickness, the free spectral range of the Cr^{2+}:ZnS microchip laser was $\Delta\nu = 2\ \mathrm{cm}^{-1}$, and the output spectrum consisted of ~50 axial modes. We attempted to arrange mode control of the microchip lasers by means of a coupled-cavity arrangement, with an additional external etalon made from a plane-parallel Si plate coupled to the microchip cavity. The etalon, with a thickness of 0.4 mm, was placed 1 cm from the microchip resonator. The coupled microchip and Si etalon cavities produced the spectral structure shown in traces (2) of Fig. 4. In these experiments the number of axial modes decreased to 25–35 modes for both lasers. This number can be further decreased to a single-longitudinal-mode oscillation in a double-cavity configuration by use of a narrow-band output coupler with a large free spectral range external etalon, as was successfully demonstrated for Tm:YLF.[14]

In conclusion, laser characterization of diffusion-doped Cr^{2+}:ZnS and Cr^{2+}:ZnSe crystals synthesized by chemical transport reaction from gas phase has been studied under cw Er-doped fiber laser excitation. For the first time to our knowledge, cw lasing of a Cr^{2+}:ZnS crystal was realized in a hemispherical cavity, with a slope efficiency of 18% with respect to the absorbed power. The key results are the first successful demonstrations of cw Cr^{2+}:ZnS and Cr^{2+}:ZnSe microchip lasers with maximum output powers of 63 and 100 mW at 2320 and 2520 nm and slope efficiencies of 53% and 20%, respectively. Further optimization of these low-cost, flexible microchip lasers will certainly stimulate new applications such as field-portable spectroscopy systems for scientific, commercial, medical, and military applications.

We thank Valentin Gapontsev and Denis Gapontsev for fruitful discussions and for providing the Er fiber laser used in this work.

References

1. L. D. DeLoach, R. H. Page, G. D. Wilke, S. A. Payne, and W. F. Krupke, IEEE J. Quantum Electron. **32,** 885 (1996).
2. R. H. Page, K. I. Schaffers, L. D. DeLoach, G. D. Wilke, F. D. Patel, J. B. Tassano, S. A. Payne, W. F. Krupke, K. T. Chen, and A. Burger, IEEE J. Quantum Electron. **33,** 609 (1997).
3. K. Graham, S. B. Mirov, V. V. Fedorov, M. E. Zvanut, A. Avanesov, V. Badikov, B. Ignat'ev, V. Panutin, and G. Shevirdyaeva, in *Advanced Solid State Lasers*, S. Payne and C. Marshall, eds., Vol. 50 of OSA Trends in Optics and Photonics Series (Optical Society of America, Washington, D.C., 2001), p. 561.
4. K. Graham, S. Mirov, V. Fedorov, M. E. Zvanut, A. Avanesov, V. Badikov, B. Ignat'ev, V. Panutin, and G. Shevirdyaeva, Proc. SPIE **4267,** 81 (2001).
5. G. J. Wagner, T. J. Carrig, R. H. Page, K. I. Schaffers, J. O. Ndap, X. Ma, and A. Burger, Opt. Lett. **24,** 19 (1999).
6. T. J. Carrig, G. J. Wagner, A. Sennaroglu, J. Y. Jeong, and C. R. Pollock, in *Advanced Solid State Lasers*, H. Ingeyan, U. Keller, and C. Marshall, eds., Vol. 34 of OSA Trends in Optics and Photonics Series (Optical Society of America, Washington, D.C., 2000), p. 182.
7. A. V. Podlipensky, V. G. Shcherbitsky, N. V. Kuleshov, V. I. Levchenko, V. N. Yakimovich, M. Mond, E. Heumann, G. Huber, H. Kretschmann, and S. Kuck, Appl. Phys. B **72,** 253 (2001).
8. E. Sorokin, I. T. Sorokina, and R. H. Page, in *Advanced Solid State Lasers*, S. Payne and C. Marshall, eds., Vol. 50 of OSA Trends in Optics and Photonics Series (Optical Society of America, Washington, D.C., 2001), p. 101.
9. U. Hommerich, X. Wu, V. R. Davis, S. B. Trivedi, K. Grasza, R. J. Chen, and S. Kutcher, Opt. Lett. **22,** 1180 (1997).
10. J. McKay, D. Kraus, and K. L. Schepler, in *Advanced Solid State Lasers*, H. Injeyan, U. Keller, and C. Marshall, eds., Vol. 34 of OSA Trends in Optics and Photonics Series (Optical Society of America, Washington, D.C., 2000), p. 219.
11. J. J. Zayhowski and A. Mooradian, Opt. Lett. **14,** 24 (1989).
12. D. Findlay and R. A. Clay, Phys. Lett. **20,** 2777 (1966).
13. J. A. Caird, S. A. Payne, P. R. Staver, A. J. Ramponi, L. L. Chase, and W. F. Krupke, IEEE J. Quantum Electron. **24,** 1077 (1988).
14. J. Izawa, H. Nakajima, H. Hara, and Y. Arimoto, Opt. Commun. **145,** 98 (1998).